

## Preparation and characterization of the Br-HPI complex of Fe<sup>(III)</sup> and their applications for dye solar cell by synthesized $\alpha$ -Fe<sub>2</sub>O<sub>3</sub> nanoparticles in a novel method

Kamal Rashid Hsejan Al- Jorani\*

\* Wasit University, College of Science, Department of Chemistry. Iraq

تحضير وتشخيص معقد الحديد مع ليكاند Br-HPI وتطبيقاته في توليف الخلية الصبغية الشمسية بواسطة جسيمات نانوية لألفا أكسيد الحديد الثلاثي بطريقة حديثة

كمال حسين شيجان  
جامعة واسط/ كلية العلوم/ قسم الكيمياء

### المستخلص:

تم تحضير مشتق لليكاند المحتوي على حلقة الازول الخماسية غير المتجانسة [Br-HPI] وتعقيداً مع أيون الحديد الثلاثي. تم تشخيص الليكاند بالوسائل الطيفية (طيف الأشعة تحت الحمراء، طيف الرنين النووي المغناطيسي)، بينما المعقد الصلب شُخص باستخدام (طيف الأشعة تحت الحمراء، التوصيل الكهربائي المولاري، العزم المغناطيسي). نتائج الدراسة بينت ان المعقد يتكون من ١ مول من فلز الحديد ٢ مول من الليكاند وذي شكل ثماني السطوح. المعقد الناتج تم تشيعه بطريقة حديثة تستخدم فيها خلية الأشعة فوق البنفسجية لتحضير جسيمات نانوية لالفا أكسيد الحديد الثلاثي والذي بدوره أستخدم لتوليف الخلية الصبغية الشمسية. الجسيمات النانوية تم تشخيصها باستخدام (المجهر الإلكتروني النافذ، المجهر الإلكتروني الماسح، حيود الأشعة السينية)، متوسط حجم الجسيمات النانوية ١١ الى ٢٥ نانومتر.

### Abstract

The derivative of five member heterocyclic ligand containing imidazole rings 4-bromo-2-(4,5-diphenyl-<sup>1</sup>H-imidazol-2-yl) phenol [Br-HPI] and their complex with Fe(III) are reported. This ligand was characterized by elemental analysis, FT-IR and <sup>1</sup>H NMR spectroscopy. The solid complex was characterized by IR spectra, molar conductivity and magnetic moment. The results suggest that the metal is bonded to the ligand through the phenolic oxygen and the pyridine nitrogen forming chelates with (1:2) (metal: ligand) stoichiometry, and the octahedral geometry for the complex. The complex has photolysis by novel method that using UV. cell to synthesis  $\alpha$ -Fe<sub>2</sub>O<sub>3</sub> nanoparticles. The nanoparticles have been indicate by transmission electron microscopy (TEM), X-ray diffraction (XRD), scanning electron microscopy (SEM), with average particles size in the range 11 to 25 nm. The  $\alpha$ -Fe<sub>2</sub>O<sub>3</sub> nanoparticles have been applied a photo anode to fabrication dye solar cell (ITO/ $\alpha$ -Fe<sub>2</sub>O<sub>3</sub> Np<sub>s</sub>/rodamine 6G dye/Ag nanofilme/ITO) with energy efficiency conversion about 2.5 %.

## Introduction

Nanoparticles are Zero dimensional because all the dimensions are measured within the nanoscale (less than 100 nm).

These compounds exhibit new and interesting properties that depend on the size (reducing size from macro and micro to nanoscale). Nanoparticles are widely present in the natural world as a result of photochemical reactions, volcanic activity and plants and algae. They have also been created as combustion residues and as the remains of the exhausted fuel of vehicles <sup>(1)</sup>. In comparison to the quantity of nanoparticles produced naturally or accidentally, nanoparticles synthesized for research or industrial purposes are a small minority. Iron oxide nanoparticles is one of the important oxides, which has many applications due to its non-toxicity <sup>(2-10)</sup>. There are many forms of iron oxide crystalline phases, which include: Hematite  $\alpha$ -Fe<sub>2</sub>O<sub>3</sub>,  $\beta$ -Fe<sub>2</sub>O<sub>3</sub>, Maghemite  $\gamma$ -Fe<sub>2</sub>O<sub>3</sub>, Epsilon Fe<sub>2</sub>O<sub>3</sub> and Magnetite (Fe<sub>3</sub>O<sub>4</sub>).  $\alpha$ -Fe<sub>2</sub>O<sub>3</sub> hematite is steel-gray, white to gray-white, with a bluish tint, in reflected light, with characteristic deep blood-red internal reflections while Nanocrystalline  $\alpha$ -Fe<sub>2</sub>O<sub>3</sub> is red <sup>(11)</sup>. The  $\alpha$ -Fe<sub>2</sub>O<sub>3</sub> crystal structure is a rhombohedrally centered hexagonal cell of the corundum type.  $\alpha$ -Fe<sub>2</sub>O<sub>3</sub> has a bandgap of 2.10 eV for bulk form and 2.2 eV for the nanocrystalline form, hematite is also highly resistant to corrosion, and commercially available at a relatively low cost <sup>(12)</sup>.

## Experimental

The chemicals and solvents of starting materials that used for synthesis the [Br-HPI] ligand and complex used without further purification. FT-IR spectra was recorded using (FT-IR-8400S Fourier Transform infrared spectrophotometer – SHIMADZU ) in the range (600-4000)cm<sup>-1</sup> using (KBr) discs. The <sup>1</sup>H NMR spectra was recorded by (<sup>1</sup>H-NMR 300 MHz, using DMSO). Sherwood Scientific's Magnetic Susceptibility Balances used to determine the magnetic susceptibilities. Conductivity meter Alpha-800 at 25°C was used to obtain the molar conductance of the transition metal complex.

- I) Preparation of the Ligand 4-bromo-2-(4,5-diphenyl-1H-imidazol-2-yl) phenol [Br-HPI].

This ligand (fig. 1) was obtained in a similar way to the preparation of the 2-(2-hydroxyphenyl)-4,5-diphenylimidazole (HPI) ligand (13). <sup>1</sup>H NMR (300 MHz, DMSO, TMS):  $\delta$  = 13.10 (s, 1H, NH), 8.24 (s, 1H, OH), 7.52–6.94 (m, 13H, ArH) ppm.

FT-IR (KBr, cm<sup>-1</sup>) : [3201 (O – H), 3406 (N – H), 1581 (C = N), 696 (Ar – Br)].

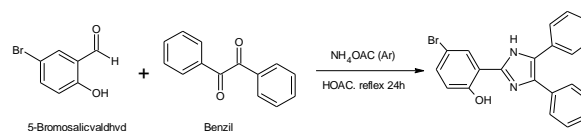
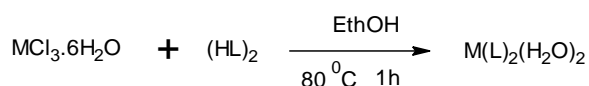


fig.(1) synthesis of [Br-HPI] ligand.

- II) Synthesis the complex of Fe(III) with [Br-HPI].

[Br-HPI] ligand (2 mmol, 0.782 gm) in ethanol (15 ml). To the solution of  $\text{FeCl}_3 \cdot 6\text{H}_2\text{O}$  (1 mmol, 0.2705 gm) in ethanol (10 ml) was added in drops. Red precipitate was formed after refluxing for 1 h and then filtered and washed with  $3 \times 30$  ml of ethanol. Yield, 1.642 gm (94 %) (fig 2).



M= Fe(III). HL= [Br-HPI]

fig (2) Complex with [Br-HPI] ligand.

### III) Synthesis of $\alpha$ - $\text{Fe}_2\text{O}_3$ nanoparticles

20 ml of 0.02 M  $[\text{Fe}(\text{Br-HPI})_2(\text{H}_2\text{O})_2]$  was irradiated by photo cell for 30 min with ice bath under  $5 \text{ C}^\circ$  (14). Orange precipitate of iron (II) complex was obtained and the product was filtered and washed several time with deionised water. The precipitate was dried in oven at  $60^\circ\text{C}$  for 4 h and calcined at  $450^\circ\text{C}$  for 3 h. A red nonmagnetic precipitate was obtained.

Fabrication of dye sensitizer solar cells. (13,14)

The dye-sensitized solar cell (2 X 1 X 0.1 cm) were synthesized according to the following process:-

A colloidal solution of  $\alpha$ - $\text{Fe}_2\text{O}_3$  nanoparticles had been prepared by mixing blending ethanol with iron oxide nano powder. A few drops of the colloid was used to cover the conductive side of ITO glass (85 % transmittance,  $8\Omega$ ), then the coated ITO glass was heated up to  $250^\circ\text{C}$  for 20 min in air to obtain the photo anod.

Later and when photo anod was cooled,  $\alpha$ - $\text{Fe}_2\text{O}_3$  nanoparticles electrode was immersed into 0.5 mM

rhodamine 6G Dye for (24 h at R.T.). The counter electrode was coated by silver nano film on ITO glass by using vacuum thermal evaporation technique. The photo anode and counter electrode was assembled the liquid electrolyte ( $\text{I}^-/\text{I}_3^-$ ) solution drop infiltrate into the working space via capillary activity, the produced cell has been held with a binder clip as shown in Fig (3)

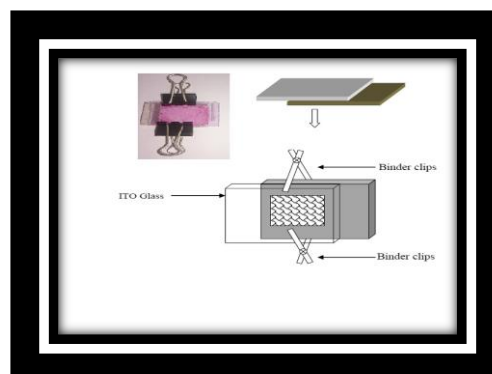


Fig (3) design of dye sensitizer solar cell.

Photocurrent –voltage behaviors of the DSSCs

A digital multimeter (proskit MT-1210) was utilized to measure the open-circuit photovoltage and short-circuit photocurrent of the DSSC. A solar stimulator with a halogen lamp and a light intensity of  $100\text{mW}/\text{cm}^2$  were employed to illuminate the dye solar cells. In addition the power conversion efficiency of the solar cell was determined by:-

$$\eta = \frac{P_{\text{max}}}{P_{\text{in}}} = \frac{V_{\text{oc}} * J_{\text{sc}} * FF}{P_{\text{in}}} * 100 \quad (2-1)$$

Where  $V_{\text{oc}}$ ,  $J_{\text{sc}}$ ,  $P_{\text{in}}$  represent the open-circuit photovoltage, the short-circuit density photocurrent and the incident light power respectively. Furthermore the fill factor is given by :-

$$FF = \frac{V_{max} \cdot J_{max}}{V_{oc} \cdot J_{sc}} \quad (2-2)$$

Where  $V_{max}$  and  $J_{max}$  represents the voltage and the current density at the maximum output power point respectively <sup>(15,16)</sup>.

Compound	Chemical Formula	Formula Weight (g·mol <sup>-1</sup> )	Color	Melting Point (°C)	Yield (%)	$\mu_{eff}$ (B.M.)	Conductivity (ohm <sup>-1</sup> ·cm <sup>2</sup> ·mol <sup>-1</sup> )
Br-HPI	C <sub>12</sub> H <sub>15</sub> N <sub>2</sub> OBr	391	white	178-180	93	-	
[Fe (Br-HPI) <sub>2</sub> (H <sub>2</sub> O) <sub>2</sub> ]	C <sub>42</sub> H <sub>32</sub> N <sub>4</sub> O <sub>4</sub> Fe	872	Red	265-268	94	4.82	3.9

## Results and Discussion

The preparation of ligand Br-HPI (fig 1) gave satisfactory analysis for the proposed structures, which was confirmed on the basis of their elemental analysis and spectral (FT-IR and <sup>1</sup>H NMR) data. The complex iron with Br-HPI ligand, were prepared by the reaction of 1:2 ratio of Metal with ligand. The complex has obtained with a good yield (94 %), insoluble in ethanol and water, but soluble in hot methanol, dimethyl sulfoxide

(DMSO). The complex is non-electrolytes in DMSO according to the conductivity measurements (Table 1). Their melting point (m.p.) and magnetic moment ( $\mu_{eff}$ ) are listed in (Table 1).

Table 1. Physical properties and Analytical data of the Br-HPI ligand and complex.

### Infrared spectra

Generally, the [Br-HPI] gives very similar IR features (Table 2). Absorption band at (3201cm<sup>-1</sup>) indicate to symmetrical stretching band of (OH) group (fig.4). The stretching band of (NH) appeared at (3406 cm<sup>-1</sup>). The vibration of Ar-Br group is observed at (696 cm<sup>-1</sup>). The band at (1581 cm<sup>-1</sup>) related to (C=N) of the (3N) imidazole nitrogen <sup>(17)</sup>. The (C=C) ring stretch, (1487, 1433 cm<sup>-1</sup>) <sup>(18)</sup>.

Coordination of the iron atom with the functional groups of the ligand was established from the IR spectra (Table 2). In general The spectra of complex show a change in frequency (fig.4,5). In addition, disappearance of the hydroxyl group stretching vibration (O-H) of Br-HPI at (3201cm<sup>-1</sup>) was observed. The Iron complex new weak bands (Table 2) appear that assign to bending vibrations of (M-O),(M-N) bonds <sup>(19-20)</sup>. The phenolic C-O stretching vibrations appeared at (1267 cm<sup>-1</sup>) in free ligand and under a shift towards lower frequencies in the complex (Table 2). This shift conforms the participation of oxygen in the C-O-M bond <sup>(21-22)</sup>. The C=N band in complex is shifted to lower frequencies, that indicated the coordination of the metal ions with (3N) imidazole nitrogen. Important

bands has been observed in the bending vibration at (1641  $\text{cm}^{-1}$ ) and stretching vibration at (3735  $\text{cm}^{-1}$ ) in Iron complex, these bands provide evidence of the existence of water molecules within the complex structure (23).

Compound	U O - H	U N - H	U C = N	U A r- B r	U (ph eno lic C- O)	U ( ( M - N )	U ( ( M - O )	U (H 2 O)
Br-HPI	3 2 0 1	3 4 0 6	1 5 8 1	6 9 6	126 7	-- --	-- --	---
Fe complex	---	3 3 0 5	1 4 8 5	7 0 0	124 8	5 4 2	4 6 3	16 41 37 35

Table 2. IR spectra of the free Br-HPI ligand and the Cu (II), Co(II) coordination complexes.

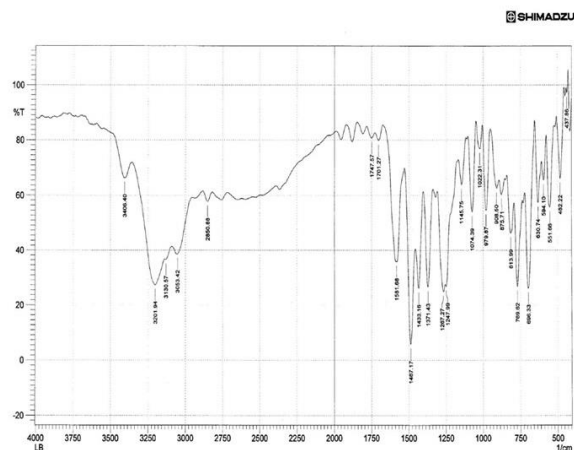


Fig.(4) : FTIR for Br-HPI ligand.

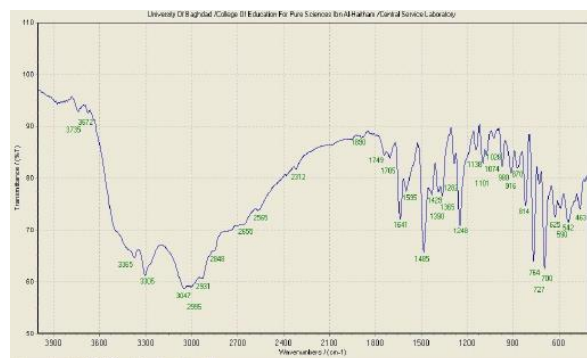


Fig. (5) : FT-IR for Fe(III) complex.

<sup>1</sup>H NMR spectra of the compounds

The <sup>1</sup>H NMR spectra of the ligand Br-HPI were obtained in d<sub>6</sub> - DMSO at room temperature using TMS as an internal standard (fig.6) The <sup>1</sup>H-NMR data Showed δ (ppm): The chemical shift observed for the (OH) proton in the ligand 8.24 (s, 1H). The 7.52–6.94 (m, 13H) for aromatic protons. While (NH) proton appeared in 13.10 (s, 1H).

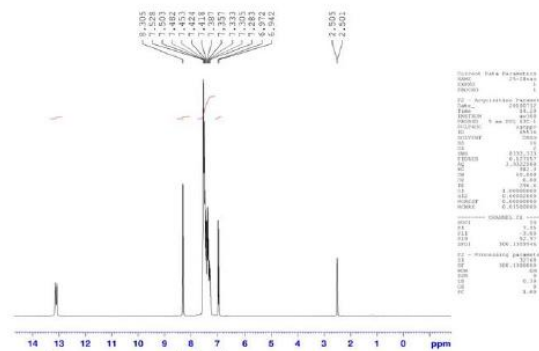


Fig. (6) : <sup>1</sup>H NMR of Br-HPI.

The morphological, structural and optical properties of synthesized  $\alpha\text{-Fe}_2\text{O}_3$  Nps were examined by various techniques. The XRD patterns of the  $\alpha\text{-Fe}_2\text{O}_3$  nanoparticles use (Cu K $\alpha$  radiation line of wavelength of 1.54 Å in 2 $\theta$  range from 10° to 80°) was shown in Figure (7).

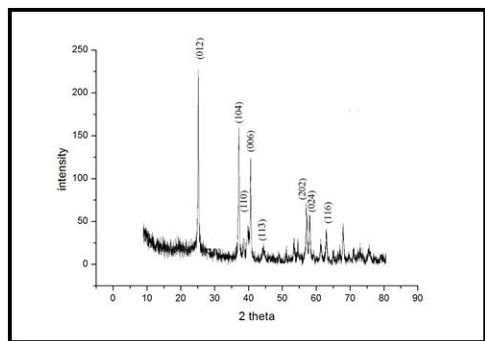


Fig. (7): XRD  
Pattern of  $\alpha$ -Fe<sub>2</sub>O<sub>3</sub> Nps (hematite)

There are significant amounts of broadening lines which are characteristic of nanoparticles. The crystal size can be calculated according to Debye-Scherrer formula<sup>(24)</sup>.

$$D = \frac{k \lambda}{\beta \cos \theta} \quad (3-1)$$

Where  $k=0.9$  scherrer constant,  $\lambda$  is the wavelength of the Cu-K $\alpha$  radiations,  $\beta$  is the full width at half maximum and  $\theta$  is the angle obtained from  $2\theta$  values corresponding to maximum intensity peak in XRD pattern. The mean crystal size of nanoparticles were 25.1 nm.

The samples in (fig.7) show the formation of  $\alpha$ -Fe<sub>2</sub>O<sub>3</sub>, based on the comparison of their XRD patterns with the standard pattern of  $\alpha$ -Fe<sub>2</sub>O<sub>3</sub> (JCPDS 33-0664) of rhombohedral structure and The diffraction peaks corresponding to (012),(104),(110),(006),(113),(202) are quite identical to characteristic peaks of the  $\alpha$ -Fe<sub>2</sub>O<sub>3</sub> crystal with the rhombohedral spinal structure. The application of Scherrer's formula to the (012) reflection peak indicated the formation of  $\alpha$ -Fe<sub>2</sub>O<sub>3</sub>.

The morphology and particles size have determined by TEM,(fig.8). The

mean particle size and distribution were determined randomly on the TEM image, (fig.8) shows TEM image of the samples. The mean particles size were obtained from TEM image was 11 nm.

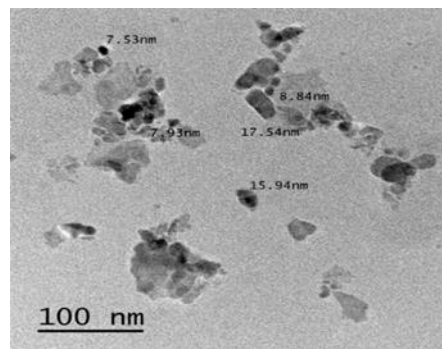


Fig. (8): TEM images of  $\alpha$ -Fe<sub>2</sub>O<sub>3</sub> NPs (hematite)

SEM images, fig (9) shows the morphology and size distribution of  $\alpha$ -Fe<sub>2</sub>O<sub>3</sub> nanoparticles. The surface of nanoparticles is smooth with good crystallinity. The average particle size and distribution were determined randomly on the SEM images. The mean particles size was obtained from SEM image 20 nm.

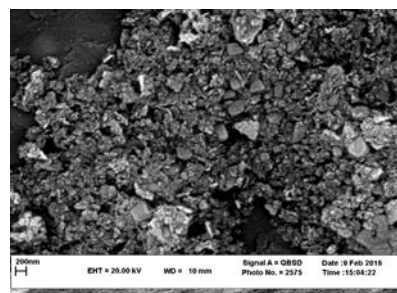


Fig. (9): SEM images of  $\alpha$ -Fe<sub>2</sub>O<sub>3</sub> NPs (hematite)

### Photovoltaic properties of dye-sensitized solar cells

Fig (10) shows the photovoltaic properties of DSSCs based on  $\alpha$ -Fe<sub>2</sub>O<sub>3</sub> NPs as a working electrode. Table (3)

summarizes the photovoltaic parameters of sample has 2.5 % energy conversion efficiency. From the I-V characteristics it is noticed that our DSSC has high the short circuit current and high open circuit voltage. This is because of the molecular structure (favourable for the separation of electron/hole pairs) and the diffusion rate of redox electrolyte.

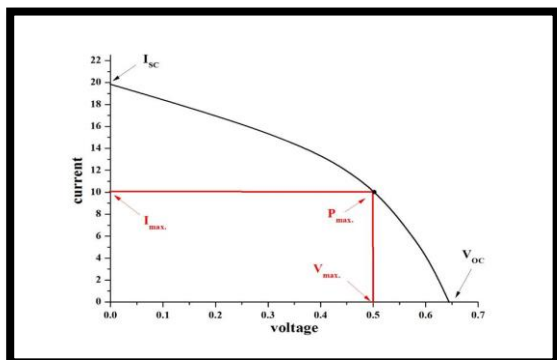


Fig. (10): photovoltaic properties of the DSSC prepared by  $\alpha$ -Fe<sub>2</sub>O<sub>3</sub> NPs

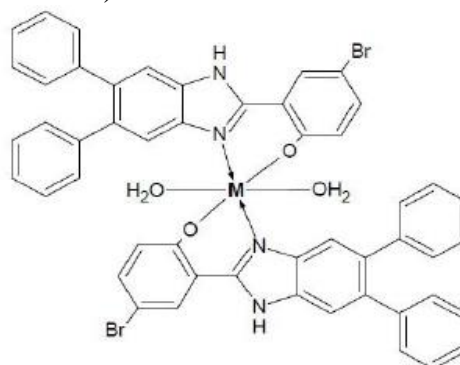
ph as e	V oc (V)	J SC (A\c m <sup>2</sup> )	V m ax (V )	J m ax (A\c m <sup>2</sup> )	P max (W\c m <sup>2</sup> )	FF	$\eta$ %
$\alpha$ - Fe 2O 3	0. 64 1	0.0 10	0. 5 0	0.0 05	0.00 25	0. 39 0	2 .5 %

Table 3. The parameters of dye sensitizer solar cell (ITO/ iron oxide Nps/ Dye (Rhodamine 6 G) /iodine / Ag film/ ITO)

### Conclusions

In conclusion, a one of easily accessible metal complex bearing Br-HPI ligand was synthesized and characterized. Obtained from the reaction of the bidentate (N, O) ligand with Fe(III) transition metal. On the basis of the physical and spectral data

of the ligand and the complex discussed above, the Br-HPI ligand is bonded to the metal via pyridine nitrogen and hydroxy group, the solid complex with the ratio [M:L] as [1:2], gives a neutral, octahedral geometry (fig. 11). Photo Irradiation process is a perfect and a novel method for preparing  $\alpha$ -Fe<sub>2</sub>O<sub>3</sub> nanoparticles. The systematic analysis for the estimate the structural properties of synthesized nanoparticles has been studied by XRD, SEM, TEM, and UV-visible, these techniques demonstrated that the nanoparticles size was less than 29 nm. The fabricated solar cell has been suitable for : (ITO/ iron oxide Nps/ Dye (Rhodamine 6 G) /iodine / Ag film/ ITO).



M=Fe (III).

Fig. (11): Complex with [Br-HPI] ligand.

### Notes and references

- 1- J. L. Elechiguerra, J. L. Burt, J. R. Morones, A. C. Bragado, X. Gao, H. H. Lara and M. J. Yacaman, Journal of Nanobiotechnology, NO. 3 PP: 1-10, (2005) .
- 2- F. Y. Cheng, C. H. Su, Y. S. Yang, C. S. Yeh, C. Y. Tsai, C. L. Wu, M. T. Wu, D. B. Shieh; Biomater., No.26, P:729, (2005).

- 3- **M. Vallet-Regi, C. V. Ragel, A. Salinas;** J. Eur. J. Inorg. Chem., p:1029, (2003).
- 4- **L. Levy, Y. Sahoo, K. S. Kim, E. Bergey;** J.Chem. Mater., No.14, p:3715, (2002).
- 5- **D. Steinhoff, U. Mohr, S. Hahnemann;** Exp. Pathol., No.43, p:189, (1991).
- 6- **A.G. Duret;** J. Phys. Chem. B, No.36, p: 17184, (2005).
- 7- **C.J. Sartoretti, M.Ulmann, B.D. Alexander, J. Augustynski, A. Weidenkaff;** J. Chem. Phys. Lett., No.376, p: 194, (2003).
- 8- **B. William, J. Ingler, U. M.Shahed, S. Khan;** J. Am. Chem. Soc., Vol.(126), No.10, p: 238, (2004).
- 9- **Chen, J.; Xu, L. N.; Li, W. Y.; Gou, X. L.** Adv. Mater., no. 17, p: 582 (2005).
- 10- **X. L. Hu, J. C. Yu, J. M. Gong, Q. Li, G. S. Li;** J. Adv. Mater., No.19, p: 2324, (2007)
- 11- **Y. Ling, G. Wang, D. A. Wheeler, J. Z. Zhang, Y. Li;** J. Nano Lett., No. 11, p: 2119, (2011).
- 12- **U. Bjorksten, J. Moser, M. Gratzel;** J. Chem. Mater., No.6, p: 858, (1994).
- 13- **K. Rsheed Al-Jourany, F. Najj. Al-Obaidi;** Iraqi National Journal of Chemistry,(2012),volume 45 ,86-104.
- 14- **D. H. Hussain, H. I. Abdulah, and A. M. Rheima;** University of AL-Mustansiriya; International Journal of Scientific and Research Publications, Volume 6, Issue 10, October (2016)
- 15- **J. P. Gonzalez,** , A Thesis Presented to the Faculty of San Diego State University, (2013).
- 16- **J. ROY-MAYHEW,** thesis for DEGREE OF DOCTOR ;CHEMICAL AND BIOLOGICAL ENGINEERING, (2013).
- 17- **Papia D., Dibakar S., Rajat S., Tapan K. Mondal, Chittaranjan S.** "Structure, photophysics, electrochemistry and DFT calculations of [RuH(CO)(PPh<sub>3</sub>)<sub>2</sub> (coumarinyl-azo-imidazole)] Polyhedron, 83, 113–211, 2113.
- 18- **Robert M. silverstein, Francis X. Webster** "spectrometric identification of organic compounds" sixth edition, 87-89, (1996).
- 19- **Muhammed B.U., Damodaran K. B. and Krishnannair K.,** "Heteroarylazo derivatives of cyclohexane-1,3-dione and their metal complexes" J. Serb. Chem. Soc.15 (1)1-13, 8811, 2113.
- 20- **Gajanan P., Narang K.,** "Synthesis, characterization, spectral studies and antifungal activity of Mn(II), Fe(II), Co(II), Ni(II), Cu(II) and Zn(II) complexes with 2-(4-sulphophenylazo)-1,5-dihydroxy-3,6-naphthalene disulphonic acid trisodium salt". Bioinorg Chem Appl., Vol. 3, Nos. 3- 4, 2118.
- 21- **S. Sarawat, G.S. Srivastava and R.C. Mehrotra.** J. Organomet. Chem. 129, 155-161 (1977).
- 22- **G. Wang and J.C. Chang.** Synth. Inorg. Met. {Org. Chem. 24, 1091-1097 (1994).
- 23- **M. Rrichenbacher and J. Popp.** challenges in molecular structure determination, 108-109, (2012).
- 24- **M. A. ahmad , A. Rahdar, F. Sadeghfar, S. Bagheri, M. R. Hajinezhad;** Nanomed Res J, Vol. 1, No.1, pp: 39-46,( 2016).